HHS Public Access

Author manuscript

Biochemistry. Author manuscript; available in PMC 2017 November 22.

Published in final edited form as:

Biochemistry. 2016 November 22; 55(46): 6363–6374. doi:10.1021/acs.biochem.6b00635.

O_2 activation by non-heme iron enzymes

Edward I. Solomon[a,b,*], **Serra Goudarzi**[a], and **Kyle D. Sutherlin**[a]

[a]Department of Chemistry, Stanford University, Stanford, California 94305, USA

[b]SLAC National Accelerator Laboratory, Menlo Park, California 94025, USA

Abstract

The non-heme Fe enzymes are ubiquitous in nature and perform a wide range of functions involving O_2 activation. These had been difficult to study relative to heme enzymes; however, spectroscopic methods have now been developed that provide significant insight into the correlation of structure with function. This Current Topics article summarizes both the molecular mechanism these enzymes use to control O_2 activation in the presence of cosubstrates and the oxygen intermediates these reactions generate. Three types of O_2 activation are observed. First, non-heme reactivity is shown to be different from heme chemistry where a low-spin Fe^{III}-OOH non-heme intermediate directly reacts with substrate. Also, two subclasses of non-heme Fe enzymes generate high-spin Fe^{IV}=O intermediates that provide both σ and π frontier molecular orbitals that can control selectivity. Finally, for several subclasses of non-heme Fe enzymes, substrate binding to the Fe^{II} site leads to the one electron reductive activation of O_2 to an Fe^{III}-superoxide capable of H-atom abstraction and electrophilic attack.

Graphical abstract

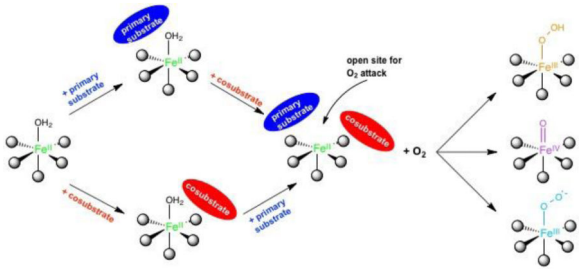

Introduction

The non-heme iron enzymes perform a wide range of critical biological functions[1,2] that include the regulation of hypoxia,[3] demethylation of DNA,[4] antibiotic and natural product biosyntheses,[5,6] and bioremediation,[7,8] are related to disease states,[9,10] and include the anticancer drug bleomycin.[11] On a molecular level these functions involve electrophilic aromatic substitution,[12] H-atom abstraction,[13] hydroxylation,[14] mono-[15] and dioxygenation,[16] ring closure[17] and expansion,[18] ring cleavage,[19] and halogenation.[20] As shown in Table 1, the mononuclear non-heme Fe enzymes divide into two classes dependent

*To whom correspondence should be addressed. Tel: 650-723-9104; edward.solomon@stanford.edu.

on whether an oxidized high-spin Fe^{III} site activates singlet organic substrates for the spin-forbidden reaction with triplet O_2 or a reduced high-spin Fe^{II} site activates O_2.

The organic substrate activating Fe^{III} sites have been considered in ref 21; here we focus on the dominant class where Fe^{II} activates O_2. These enzymes generally have a facial triad of three protein-derived ligands (2 His and one carboxylate),[22] with additional H_2O-derived ligands completing the Fe^{II} coordination, although the halogenases have the carboxylate replaced by a halide[23] and several enzymes (including diketone-cleaving dioxygenase and cysteine dioxygenase) have the carboxylate replaced by a third His ligand.[24]

The Fe^{II} enzymes in Table 1 are subdivided based on whether a cosubstrate or cofactor is required and the nature of the primary substrate.[2] In the pterin and α-ketoglutarate (αKG) dependent enzymes, the exogenous cosubstrate donates two electrons via the reactions given in Equation 1, while in the Rieske dioxygenases an endogenous 2Fe2S Rieske center donates one of the electrons for O_2 activation.

$$\text{Reduced pterin} + {}^{*}O_2 \rightarrow 2e^{-} + {}^{*}4\text{OH pterin} \rightarrow \text{oxidized pterin} + {}^{*}H_2O$$

$$\alpha\text{KG} + {}^{*}O_2 \rightarrow 2e^{-} + {}^{*}\text{succinate} + CO_2 \quad \text{Equation 1}$$

The next two categories of non-heme Fe enzymes in Table 1 only involve a substrate, where in the extradiol dioxygenases it is a catechol capable of two-electron oxidation to a quinone as part of the catalytic cycle, while in a fifth category the substrates are not intrinsically redox active. Finally, bleomycin is listed here as the Fe^{II} site of this glycopeptide antibiotic binds O_2 and is further reduced by one exogenous electron to generate activated bleomycin,[25] the intermediate kinetically competent to cleave DNA by H-atom abstraction in its anticancer function.

The high-spin Fe^{II} active sites in these enzymes had been spectroscopically inaccessible due to their lack of the π to π* transitions of heme enzymes.[26] Thus a new spectroscopic methodology was developed (variable-temperature variable-field magnetic circular dichroism, VTVH MCD)[1] that elucidated a general mechanistic strategy utilized by many of the different non-heme Fe^{II} enzymes in Table 1 that is summarized in Section 1. O_2 intermediates have thus far been clearly observed in bleomycin,[25] the αKG and pterin dependent enzymes,[27,28] and the extradiol dioxygenases.[29–31] A focus of our research on these intermediates has been to use nuclear resonance vibrational spectroscopy (NRVS) to define geometric structure and VTVH MCD to define electronic structure and their contributions to reactivity. The results of these studies on the Fe^{III}-hydroperoxide in activated bleomycin, the Fe^{IV}=O in the αKG and pterin dependent enzymes, and the possible involvement of an Fe-$O_2^{\bullet-}$ intermediate in several subclasses in Table 1 are summarized in subsequent sections. These studies emphasize: 1) the difference in reactivity between non-heme and heme Fe enzymes, 2) the nature of the frontier molecular orbitals (FMOs) of Fe^{IV}=O $S = 2$ and how these can control the type of reactivity, and 3) substrate

contributions to the thermodynamically difficult one-electron reduction of O_2 to form Fe-superoxo intermediates.

1. General mechanistic strategy of non-heme Fe^{II} enzymes

Non-heme high-spin Fe^{II} active sites do not have intense absorption features, but do have weak d → d, ligand field (LF) transitions, which are characteristic of the coordination environment. Their low intensity and near IR energy region (12,000 – 5000 cm^{-1}) make the study of LF transitions in metalloproteins inaccessible by absorption spectroscopy. However, their ground states have $S = 2$ and thus are paramagnetic, which leads to high intensity in MCD spectroscopy at low temperature. As shown in Figure 1A, the low temperature (LT) MCD spectra of Fe^{II} sites is characteristic of coordination number, with six-coordinate (6C) sites having two transitions at ~10,000 cm^{-1} split by ~2000 cm^{-1}, 5C square pyramidal Fe^{II} sites having transitions at >~10,000 and ~5000 cm^{-1}, 5C trigonal bipyramidal having transitions at <10,000 and <5000 cm^{-1}, and 4C distorted tetrahedral having LF transitions only at low energy (5000–7000 cm^{-1}) in LT MCD. The temperature and field dependence of the MCD data for these provide significant additional insight into the ground state of these sites, and the reader is referred to ref 1 for details.

Figure 1B demonstrates how LT MCD provided significant insight into the molecular mechanism of the Fe^{II} active site in the pterin dependent enzyme phenylalanine hydroxylase (PAH, done in collaboration with Prof. John Caradonna).[32] The resting Fe^{II} site shows two transitions at ~10,000 cm^{-1} split by ~2000 cm^{-1} (black MCD spectrum in Figure 1B), demonstrating that it is 6C. Addition of the primary substrate, phenylalanine, only slightly perturbs the spectrum (blue), while addition of pterin has no effect on the MCD spectrum (green, which demonstrates that the pterin cosubstrate does not bind to the Fe^{II} center). Importantly, upon binding both phenylalanine and pterin, there is a dramatic change in the MCD spectrum showing one band at ~10,000 cm^{-1} with one at ~5000 cm^{-1} (red), indicating that the Fe^{II} has now gone 5C, opening a coordination position on the iron for O_2 activation.

Parallel experiments to those described above have been done on members of all the six subclasses of non-heme Fe^{II} enzymes in Table 1 with parallel results[32–37] that have led to the general mechanistic strategy utilized by the non-heme Fe^{II} enzymes shown in Figure 2.

The resting Fe^{II} site, the site in the presence of primary substrate, or the site with cosubstrate bound are 6C, coordinatively saturated and relatively stable in the presence of O_2. This coordination saturation is important in the presence of the reduced cosubstrate, as all electrons are present and the site is primed for O_2 reaction. Importantly, the presence of all cosubstrates opens a coordination position of the Fe^{II} for O_2 activation, enabling coupled turnover (i.e. one molecule of product for every cosubstrate).

The need for both cosubstrate and primary substrate to be present to form an open coordination position is a key advantage of the general mechanistic strategy defined by the MCD data, as it minimizes cosubstrate turnover without primary substrate. A kinetic model for the αKG dependent dioxygenases is given in Scheme 1.

The enzyme first reversibly binds cosubstrate (C) or primary substrate (S) to form 6C complexes, important in preventing activation of O_2 by the EC complex in the absence of primary substrate. The binding of both cosubstrates results in a 5C ECS complex that can now react with O_2. In TauD, binding of the primary substrate significantly enhances the binding affinity of αKG, reducing K_D by an order of magnitude.[38] Although it is unclear whether O_2 binds reversibly before the irreversible reaction in the ECS complex,[39] saturation behavior with increasing concentrations of O_2 is observed.[40] The only intermediate observed in the reaction with O_2 is the Fe^{IV}=O complex (I) that results from αKG decarboxylation, and its formation and decay to the product complex (EP) have been observed in multiple αKG and pterin dependent enzymes.[27,28,41–43] The general mechanistic strategy has the advantage of requiring primary substrate to be present when I is formed, which minimizes unproductive decay channels that include self-hydroxylation and auto-oxidation reactions that inactivate the enzyme.[44] Indeed, KIE experiments that increase the accumulation of I show a marked increase in these unproductive decay pathways.[27] Note that there had been a “booby-trapped” mechanism proposed for DAOCS where the EC complex was thought to react with O_2 to generate a stable peroxy intermediate.[45] However, a number of calculations and experiments have demonstrated that the peroxy is at higher energy relative to the Fe^{IV}=O,[46,47] which is the only intermediate observed.[27] Also it has been shown that DAOCS does, in fact, form a ternary complex in line with the general mechanistic strategy presented above.[48]

Insight has been derived into the molecular basis for the 6C → 5C conversion in the presence of cosubstrate and primary substrate and into the role of the facial triad and its second sphere residues in this conversion. As shown in Figure 2, the 6C → 5C conversion with primary substrate and cosubstrate involves loss of a H_2O ligand. The identity of the lost ligand upon binding of both cosubstrates was determined by crystallography for the αKG dependent enzymes[49] and with EXAFS for the pterin dependent NHFe enzymes.[50] The factors driving water ligand loss were evaluated in the αKG dependent enzyme, factor inhibiting HIF-1 (FIH) in collaboration with Prof. Mike Knapp. In the presence of only cosubstrate, electron donation by the αKG, which coordinates the Fe^{II} in a bidentate mode, weakens the Fe^{II}-OH_2 bond based on LF changes from VTVH MCD.[51] (This strong donor interaction is also present in the extradiol dioxygenases that coordinate a catecholate substrate bidentate, as well as in the enzymes that react with non-redox active substrates like isopenicillin-N synthase, IPNS.) However, the water remains bound due to hydrogen bonding between the unbound oxygen of the monodentate carboxylate ligand of the facial triad and the water. Further addition of primary substrate, which does not directly coordinate Fe^{II} but binds in the active site pocket, destabilizes the 6C site due to steric interactions with the coordinated water. In FIH, primary substrate binding also stabilizes the 5C site through hydrogen bonding between the substrate and the unbound oxygen of the carboxylate thereby weakening the carboxylate-water H-bond. These effects are shown in Figure 3.

Second sphere residues are also important in preserving the reactivity of the 5C site with O_2. In FIH, a second sphere arginine (R238) maintains the monodentate coordination of the facial triad carboxylate ligand by H-bonding to the unbound oxygen. DFT calculations predict that removal of this H-bonding interaction would result in the facial triad carboxylate binding bidentate,[51] which would eliminate the open coordination position for O_2 binding.

Indeed, activity in the R238M FIH mutant is reduced to 5% of WT.[52] Importantly, in enzymes that coordinate a cosubstrate or primary substrate bidentate to the Fe^{II} (αKG dependent enzymes and the extradiol dioxygenases), a second sphere residue is present that provides an H-bond to stabilize a monodentate carboxylate, critical in maintaining an open coordination position for O_2 activation. Note that in the NHFe enzymes that do not have the bound primary substrate or cosubstrate occupy two coordination positions (pterin dependent and Rieske dioxygenases), there is no second sphere H-bond and the carboxylate goes bidentate still leaving open coordination positions for O_2 activation, as shown in Figure 4.

As mentioned above, three types of oxygen intermediates have been identified in the different subclasses of O_2 activating non-heme Fe enzymes. In the sections below, we consider each of these and its activation in terms of frontier molecular orbital (FMO) theory.

2. The low spin $Fe^{III}OOH$ intermediate in bleomycin: non-heme vs heme reactivity

While activated bleomycin (ABLM) had been thought to be a low-spin Fe^{III}-hydroperoxide, a computational study raised issues that lead to its further elucidation.[53] Normally, resonance Raman spectroscopy would be used to identify the nature of an axial ligand; however, ABLM is unstable in the laser beam,[54] so NRVS was employed.[55] This experiment requires a third-generation synchrotron where the^{57}Fe nuclear Mössbauer transition is scanned to higher energy to observe vibrational sidebands.[56,57] The resultant NRVS spectrum gives intensity at a given energy reflecting the amount of Fe motion in a vibration of the metalloenzyme at that energy. The NRVS spectra of low-spin Fe^{III} BLM and ABLM are given in Figure 5, with DFT simulations of the NRVS data given below for the structure that best agrees with the data.

Ferric BLM shows a feature at 567 cm^{-1} that shifts with $H_2{}^{18}O$. The high energy of this stretch of the water derived ligand shows that low-spin Fe^{III} BLM has a hydroxide-Fe^{III} axial ligand. The intense feature at 400 cm^{-1} is a degenerate pair of transaxial bends. In going to ABLM (Figure 5B), these split by 40 cm^{-1} and there is a low-energy 328 cm^{-1} peak. This can only be simulated with a low-spin $Fe^{III}OOH$ where the 328 cm^{-1} feature is the OOFe bend and this couples to the in-plane transaxial bend (Figure 5C), which leads to the split spectral features.

Thus, ABLM is a low-spin $Fe^{III}OOH$, which is the non-heme Fe equivalent of compound 0 in p450. As shown in equation 2A, it has been determined in p450 that the $Fe^{III}OOH$ protonatively cleaves to generate compound *I*,[58,59] an Fe^{IV}=O with a one electron oxidized porphyrin ring.

$$Fe^{III}(Por)(SCH_3)-OOH+H^+ \rightarrow Fe^{IV}O(Por^{\bullet+})+H_2O \quad \Delta G=-58 kcal/mol \quad \text{Equation 2A}$$

$$Fe^{III}(BLM)-OOH+H^+ \rightarrow Fe^{V}O(BLM)+H_2O \quad \Delta G=+13 kcal/mol \quad \text{Equation 2B}$$

$$Fe^{III}(BLM)-OOH+RH \rightarrow Fe^{IV}O(BLM)+R^{\bullet}+H_2O \quad \Delta G=-7kcal/mol$$ Equation 2C

For p450, this is a highly exergonic reaction calculated to be −58 kcal/mol for a proton from solvent.[60] If the same calculation is done on ABLM (equation 2B), the reaction is 71 kcal/mol less favorable and is endergonic by at least 13 kcal/mol with the same source of proton.[61] This energy difference reflects the fact that it is much harder to oxidize a non-heme relative to a heme ligand where the hole is delocalized over the porphyrin ring and further stabilized by its negative charge.

Alternatively, if the low-spin $Fe^{III}OOH$ is directly reacted with the H-C bond of a substrate modeling DNA, the reaction is exergonic by 7 kcal/mol (equation 2C).[62] This direct reaction of the Fe^{III}-hydroperoxide with DNA was studied experimentally,[62] using CD to monitor the kinetics of the decay of ABLM. It was determined that DNA accelerated the rate of decay of ABLM and defined it as having a small primary and large secondary KIE. These experimental data were computationally modeled and found to reflect the transition state in Figure 6A, which is late in O-O cleavage and early in H-atom abstraction. This leads to consideration of the FMO of a low spin $Fe^{III}OOH$, Figure 6B, which is the peroxo σ^* orbital. Upon elongation of the O-O bond to the late transition state, the σ bonding is essentially lost and the two electron holes in the σ^* polarize, one on the distal O generating a hydroxyl directed toward the C-H bond of the substrate, and the other to the proximal O generating an Fe^{IV}=O capable of a second H-atom abstraction, also with a low barrier, leading to double strand cleavage, important in the anticancer activity of the drug.[64]

3. Fe^{IV}=O Intermediates: frontier molecular orbital control of reactivity

Iron-oxo intermediates have been trapped and defined in a series of αKG and pterin dependent enzymes (syringomycin biosynthesis enzyme 2 [SyrB2],[20] taurine dioxygenase [TauD],[27] prolyl 4-hydroxylase [P4H],[43] CytC3,[41] tyrosine hydroxylase [TH],[28] and PAH][42]). From EXAFS on the TauD intermediate J, the Fe-O bond length is 1.62 Å,[65] and from resonance Raman on this intermediate the $\nu_{Fe\text{-}O}$ is 821 cm^{-1}.[66] Mössbauer studies have been done on all the intermediates listed above giving δ = 0.22 – 0.30 mm/s and $|\Delta E_Q|$ = 0.76 – 1.27 mm/s, and importantly, from magnetic Mössbauer, the ground state is high-spin with $S = 2$.[67,68] In order to obtain detailed geometric structural insight into an Fe^{IV}=O intermediate in an enzyme system, NRVS was done on the halogenase SyrB2 in collaboration with Professors Krebs and Bollinger, where both the Cl^- and Br^--bound forms (replacing the carboxylate of the facial triad) could be studied, enabling a perturbation of the spectral features.[69] From the data in Figure 7, the NRVS spectrum of SyrB2 has three peaks where the intensity shifts from the high to the low energy region with $Cl^- \rightarrow Br^-$.

This is an interesting mass effect where the heavy Br^- shifts iron motion into the low energy vibrations. These data were correlated to a range of possible structural models using experimentally calibrated DFT methods, and one structure reproduced the three-peak pattern and shift of intensity with Br^-. This is a 5-coordinate trigonal bipyramidal structure with the Fe-O bond along the approximate C_3 axis of this intermediate (Figure 7, bottom).

The geometric and electronic structure of this enzyme intermediate[70] are very similar to those of a structurally defined model complex, $[Fe^{IV}(O)(TMG_3tren)]^{2+}$, of Que et al.[71,72] Variable temperature MCD spectroscopy on this model (and the enzyme intermediate) then provided detailed electronic structural insight, and in particular, combined with calculations, defined the FMOs available for electrophilic reactivity.[73] The correlation of the MCD data to the absorption data in Figure 8A revealed and assigned key excited states which correspond to the transitions in Figure 8B: the $d\pi^* \rightarrow d\sigma^*$ ligand field transitions involving two key FMOs and an oxo π to $d\pi$ ligand to metal charge transfer (CT) transition defining a third oxo π^* FMO.

Multireference CASPT2 calculations were correlated to the spectral data in Figure 8A and extended to the elongated Fe-O transition state (1.81 – 1.84 Å) associated with its reactivity. From Figure 8C, these studies reveal three very reactive FMOs: a σ^* FMO oriented along the Fe-O bond with significant oxo p_z σ^* character for reacting along this bond and two π^* FMOs with oxo $p\pi$ character activated for reaction perpendicular to the Fe-O bond. Further, it was found that near the transition state all three FMOs gain a great deal of oxo hole character, effectively becoming Fe^{III}-oxyl sites for enhanced reactivity.

These π and σ FMOs and their orientation dependence, present only in $S = 2$ Fe^{IV}=O non-heme intermediates, provide an electronic mechanism to control reactivity. Two systems that appear to utilize these FMOs to enable reactivity are presented below.

(4-hydroxyphenyl) pyruvate dioxygenase (HPPD) and (4-hydroxy) mandelate synthase (HmaS) both react with the same substrate, (4-hydroxyphenyl) pyruvate (HPP), but with different outcomes of the reaction: electrophilic attack on the ring in the former and H-atom abstraction of the benzylic H in the latter. Spectral studies have shown that HPP (where the α-keto acid is covalently linked to the substrate) binds to the Fe with different conformations of the ring.[74,75] Extension to the decarboxylated Fe^{IV}=O intermediate in Figure 9 showed that, for HPPD, the ring can be oriented for σ^* FMO attack on its π electron cloud, while for HmaS with the ring oriented away from the site the Fe=O is still reactive in H-atom abstraction using its π^* FMO, perpendicular to the Fe-O bond.[76]

For the halogenase SyrB2 mentioned above, reaction of the native substrate leads to selective halogenation, while reaction with alternative substrates can lead to hydroxylation,[77] which is thermodynamically favored. Following the reaction coordinate in Figure 10, O_2 binding to the 5C Fe^{II} activates it for nucleophilic attack on the carbonyl C, the CO_2 is lost, and the O-O bond cleaves. For the native substrate this leads to the 5C ~C_3 trigonal bipyramidal Fe^{IV}=O structure as found from the NRVS data in Figure 7, importantly with the Fe-O bond perpendicular to the H-C bond of the substrate.[69] From this orientation, the Fe^{IV}=O is still capable of H-atom abstraction with a reasonable barrier due to its active π^* FMO. This leads to an Fe^{III}-OH first intermediate with the OH group oriented away from the carbon radical of the substrate, but with the halide well-oriented for rebound halogenation. Thus the $S = 2$ of the Fe^{IV}=O intermediate in NHFe enzymes has both π and σ FMOs (in contrast to the Fe^{IV}=O intermediate in heme enzymes with an $S = 1$ ground state,[78] which has only a π FMO[79]) that can provide important flexibility and control of oxo reactivity in biology.

5. Fe^{III}-$O_2^{\bullet-}$ intermediates: one electron reductive activation of O_2

High-spin Fe^{III}-$O_2^{\bullet-}$ species have been invoked as the intermediate that reacts directly with substrate in three subclasses of NHFe enzymes: the non-redox active substrate enzymes (that include IPNS), the extradiol dioxygenases, and recently, the Rieske dioxygenases.[80–82] Of these, direct experimental evidence for the formation of a Fe^{III}-$O_2^{\bullet-}$ intermediate has only been reported in the extradiol dioxygenase homoprotocatechuate 2,3-dioxygenase (HPCD)[29,81] and, recently, in IPNS.[83] Defining the factors that enable the one-electron reduction of O_2 by a high-spin Fe^{II} site is fundamental in understanding the reactivities of these subclasses of O_2-activating mononuclear NHFe enzymes.

It is important to note that, from MCD and crystallography, the resting Fe^{II} active site is five-coordinate square pyramidal (facial triad plus two H_2O ligands) in two type I extradiol dioxygenases, 2,3-dihydroxybiphenyl 1,2-dioxygenase (DHBD)[84,85] and catechol 2,3-dioxygenase (CTD).[86,87] Thus, even in the absence of substrate, the resting active site is coordinatively unsaturated, yet these resting Fe^{II} enzymes are relatively stable in the presence of O_2. A computational study gave results consistent with this observation, finding that O_2 binding to the resting 5C facial triad site of DHBD was highly endergonic.[35] An experimentally calibrated functional (BP86 with 10% Hartree-Fock exchange) gives an endergonic free energy of 19 kcal/mol (Figure 11 right, blue).[36] Three factors contribute to the reaction of O_2 with the 5C facial triad being unfavorable. First, the one-electron reduction potential of O_2 to superoxide is low (−0.16 V in aqueous solution),[88] and the Fe^{II}/Fe^{III} reduction potential for a facial triad is high (+0.19 V for PAH, which represents a lower limit as PAH is 6C)[89] due to the poor donor ability of the facial triad ligation. In addition, binding of O_2 to an open coordination site leads to an entropic penalty of 10–12 kcal/mol at room temperature.[90] Finally, the Fe^{III}-$O_2^{\bullet-}$ bond is relatively weak. This can be seen in the computational comparison of the energetics of the binding of O_2 and NO to a facial triad site (Figure 11). The one electron reduction of NO to NO^- (red line center, Figure 11) is more difficult than that of O_2 to O_2^- (blue line) by ~5 kcal/mol, yet NO binding is more favorable by 25.9 kcal/mol due to the strong Fe-N bond (length = 1.74 Å) relative to the weaker Fe-O bond (1.87 Å).[36]

In all of the three subclasses of NHFe enzymes invoking superoxide intermediates, substrate binding to the active site turns on the O_2 reactivity. The origin of this substrate activation was evaluated in collaboration with Prof. John Lipscomb for a member of the non-redox substrate enzyme subclass, IPNS, where the substrate bound to Fe cannot provide additional electrons.[36] IPNS binds its substrate, δ-(l-α-aminoadipoyl)-l-cysteinyl-d-valine (ACV), monodentate through its cysteinyl S and catalyzes the formation of isopenicillin-N through an initial H-atom abstraction step.[91] DFT calculations found that O_2 binding to the 5C IPNS-ACV site was now exergonic by 7 kcal/mol (Figure 11 right, purple line), relative to +19 kcal/mol for O_2 binding to the resting facial triad site (Figure 11, blue line). From MCD spectroscopy on the stable nitrosyl analogue of the putative Fe^{III}-ACV-$O_2^{\bullet-}$ complex, a new low energy transition is present that is assigned as a substrate thiolate π to Fe^{III} 3d charge transfer. This reflects strong sulfur donation that stabilizes the Fe^{III}-ACV complex relative to the resting Fe^{III} facial triad (Figure 11, middle), lowering the reduction potential and enabling the formation of an Fe^{III}-ACV-$O_2^{\bullet-}$ complex by 25.9 kcal/mol. This superoxide

Fe^{III} species has recently been identified in IPNS by Mössbauer spectroscopy.[83] Computationally, this Fe^{III}-superoxo intermediate is found to be activated by its π* FMO (Figure 12) to perform H-atom abstraction from the β methylene C of the substrate.[36]

In the extradiol dioxygenases, understanding the one-electron activation of O_2 is complicated by the presence of the redox active catecholate substrate. In these enzymes, an alkylperoxo bridge to the substrate is formed after O_2 is activated through binding to the Fe^{II} site.[92] Due to the non-innocence of the catecholate, the source of the electron for O_2 activation and thus the electronic structure of the species that attacks the aromatic ring is an open issue. On the basis of crystallographic[81] and computational[93] studies, it was proposed that the substrate activates O_2 to the superoxy level, leading to a Fe^{II}-semiquinone-$O_2^{\bullet-}$ species (Scheme 2A) that would then radical couple to form the alkylperoxo bridged species. Another possibility is that the strong charge donation from the catecholate tunes the donor potential of the Fe^{II} in a manner similar to that defined above for IPNS, leading to a Fe^{III}-catecholate-$O_2^{\bullet-}$ species that would attack the ring (Scheme 2B). This is supported by computational study[94] and by the isolation of a Fe^{III}-catecholate-superoxo species in the H200N variant of HPCD using a slow substrate,[29] though this intermediate is not active in extradiol cleavage. Another possibility is that both Fe^{II} and substrate donate an electron to O_2, leading to a Fe^{III}-semiquinone-peroxy or hydroperoxy active species (Scheme 2C), supported by Mössbauer and EPR data that suggest the formation of such an intermediate in the H200C and H200N mutants of HPCD that are active in extradiol cleavage.[30,31] More experimental data are needed to evaluate the nature of the active species in the extradiol dioxygenases and define the role of substrate in their activation of O_2.

In the Rieske dioxygenases (RDOs), which catalyze the cis-dihydroxylation of aromatic rings, the electrons necessary for the reaction are provided by the catalytic mononuclear NHFe Fe^{II} site and by a 2Fe2S Rieske cluster ~12 Å away capable of one electron donation.[95] In a peroxide shunt reaction of the RDO benzoate 1,2-dioxygenase with both the mononuclear Fe and Rieske sites oxidized and substrate bound, a high-spin Fe^{III}-(hydro)peroxy intermediate was isolated,[96] and has also been observed by crystallography.[97,98] However, the involvement of this peroxy intermediate in the O_2 activation mechanism has been called into question by a substrate dependence of the rate of Rieske oxidation, implying that an Fe^{III}-$O_2^{\bullet-}$ species that reacts with substrate to form an Fe^{III}-peroxo-aryl radical species is formed prior to oxidation of the Rieske site.[82] In the RDOs, substrate does not bind directly to the Fe site (and thus cannot tune its reduction potential), and it is not redox active. It is possible that the bidentate coordination of the facial triad carboxylate that occurs in this class of enzymes (*vide supra*) could help stabilize the formation of an Fe^{III}-$O_2^{\bullet-}$ intermediate. It is also possible that the reaction is driven by a thermodynamically favorable later step in the mechanism. The relevance of a superoxide-Fe^{III} intermediate in the RDOs must still be understood in the context of the peroxide shunt reaction as this produces the same diol product.

6. Concluding comments

Our understanding of the non-heme iron enzymes has greatly advanced through detailed mechanistic, model, spectroscopic, and crystallographic studies. However, there are still

important issues to be considered that include details of the molecular mechanism of O_2 activation, the nature of key intermediates, including the superoxo, and their electronic and steric contributions to reactivity and specificity. It is also important to understand how the mononuclear NHFe enzymes relate to the binuclear NHFe enzymes and to the heme enzymes in O_2 activation and their abilities to perform significant biochemistry.

Acknowledgments

E.I.S. would like to thank past students and collaborators for their major research contributions.

Funding statement

Funding for this work was provided by the National Institutes of Health (GM-40392 to E.I.S.).

Abbreviations

5C	5-coordinate
6C	6-coordinate
ABLM	activated bleomycin
ACV	δ-(l-α-aminoadipoyl)-l-cysteinyl-d-valine
αKG	α-ketoglutarate
BLM	bleomycin
DFT	density functional theory
EXAFS	Extended X-ray absorption fine structure
FIH	factor inhibiting HIF-1
FMO	frontier molecular orbital
HmaS	(4-hydroxy) mandelate synthase
HPCD	homoprotocatechuate 2,3-dioxygenase
HPPD	(4-hydroxyphenyl) pyruvate dioxygenase
IPNS	isopenicillin-N synthase
LF	ligand field
LT	low temperature
MCD	magnetic circular dichroism
NHFe	non-heme Fe
NRVS	nuclear resonance vibrational spectroscopy
PAH	phenylalanine hydroxylase

RDO	Rieske dioxygenase
SyrB2	syringomycin biosynthesis enzyme 2
TauD	taurine dioxygenase
VTVH MCD	variable-temperature variable-field magnetic circular dichroism

References

1. Solomon EI, Brunold TC, Davis MI, Kemsley JN, Lee SK, Lehnert N, Neese F, Skulan AJ, Yang YS, Zhou J. Geometric and electronic structure/function correlations in non-heme iron enzymes. Chem. Rev. 2000; 100:235–349. [PubMed: 11749238]
2. Solomon EI, Light KM, Liu LV, Srnec M, Wong SD. Geometric and Electronic Structure Contributions to Function in Non-heme Iron Enzymes. Accounts Chem. Res. 2013; 46:2725–2739.
3. Mahon PC, Hirota K, Semenza GL. FIH-1: a novel protein that interacts with HIF-1 alpha and VHL to mediate repression of HIF-1 transcriptional activity. Genes & Dev. 2001; 15:2675–2686. [PubMed: 11641274]
4. Falnes PO, Klungland A, Alseth I. Repair of methyl lesions in DNA and RNA by oxidative demethylation. Neuroscience. 2007; 145:1222–1232. [PubMed: 17175108]
5. Baldwin JE, Abraham E. The Biosynthesis of Penicillins and Cephalosporins. Nat. Prod. Reports. 1988; 5:129–145.
6. Vaillancourt FH, Vosburg DA, Walsh CT. Dichlorination and bromination of a threonyl-S-carrier protein by the non-heme Fe-II halogenase SyrB2. Chembiochem. 2006; 7:748–752. [PubMed: 16528784]
7. Gibson DT, Parales RE. Aromatic hydrocarbon dioxygenases in environmental biotechnology. Curr. Opin. Biotechnol. 2000; 11:236–243. [PubMed: 10851146]
8. Furukawa K. Engineering dioxygenases for efficient degradation of environmental pollutants. Curr. Opin. Biotechnol. 2000; 11:244–249. [PubMed: 10851151]
9. Scriver CR, Eisensmith RC, Woo SLC, Kaufman S. The Hyperphenylalaninemias of Man and Mouse. Annu. Rev. Genet. 1994; 28:141–165. [PubMed: 7893121]
10. Tiranti V, Viscomi C, Hildebrandt T, Di Meo I, Mineri R, Tiveron C, Levitt MD, Prelle A, Fagiolari G, Rimoldi M, Zeviani M. Loss of ETHE1, a mitochondrial dioxygenase, causes fatal sulfide toxicity in ethylmalonic encephalopathy. Nat. Med. 2009; 15:200–205. [PubMed: 19136963]
11. Chabner, BA. Cancer chemotherapy and biotherapy: principles and practice. Philadelphia, PA: Wolters Kluwer Health/Lippincott Williams & Wilkins; 2011. Bleomycin and Other Antitumor Antibiotics; p. 323-341.
12. Kovaleva EG, Lipscomb JD. Versatility of biological non-heme Fe(II) centers in oxygen activation reactions. Nat. Chem. Biol. 2008; 4:186–193. [PubMed: 18277980]
13. Costas M, Mehn MP, Jensen MP, Que L. Dioxygen activation at mononuclear nonheme iron active sites: Enzymes, models, and intermediates. Chem. Rev. 2004; 104:939–986. [PubMed: 14871146]
14. Fitzpatrick PF. Tetrahydropterin-dependent amino acid hydroxylases. Annu. Rev. Biochem. 1999; 68:355–381. [PubMed: 10872454]
15. Capyk JK, D'Angelo I, Strynadka NC, Eltis LD. Characterization of 3-Ketosteroid 9 alpha-Hydroxylase, a Rieske Oxygenase in the Cholesterol Degradation Pathway of Mycobacterium tuberculosis. J. Biol. Chem. 2009; 284:9937–9946. [PubMed: 19234303]
16. Joseph CA, Maroney MJ. Cysteine dioxygenase: structure and mechanism. Chem. Commun. 2007:3338–3349.
17. Busby RW, Townsend CA. A single monomeric iron center in clavaminate synthase catalyzes three nonsuccessive oxidative transformations. Bioorganic & Med. Chem. 1996; 4:1059–1064.
18. Lloyd MD, Lee HJ, Harlos K, Zhang ZH, Baldwin JE, Schofield CJ, Charnock JM, Garner CD, Hara T, van Scheltinga ACT, Valegard K, Viklund JAC, Hajdu J, Andersson I, Danielsson A, Bhikhabhai R. Studies on the active site of deacetoxycephalosporin C synthase. J. Mol. Biol. 1999; 287:943–960. [PubMed: 10222202]

19. Vaillancourt FH, Bolin JT, Eltis LD. The ins and outs of ring-cleaving dioxygenases. Crit. Rev. Biochem. Mol. Biol. 2006; 41:241–267. [PubMed: 16849108]
20. Matthews ML, Krest CM, Barr EW, Vaillancourt FH, Walsh CT, Green MT, Krebs C, Bollinger JM Jr. Substrate-Triggered Formation and Remarkable Stability of the C-H Bond-Cleaving Chloroferryl Intermediate in the Aliphatic Halogenase, SyrB2. Biochemistry. 2009; 48:4331–4343. [PubMed: 19245217]
21. Pau MY, Lipscomb JD, Solomon EI. Substrate activation for O2 reactions by oxidized metal centers in biology. Proc. Natl. Acad. Sci. 2007; 104:18355–18362. [PubMed: 18003930]
22. Koehntop KD, Emerson JP, Que L. The 2-His-1-carboxylate facial triad: a versatile platform for dioxygen activation by mononuclear non-heme iron(II) enzymes. J. Biol. Inorg. Chem. 2005; 10:87–93. [PubMed: 15739104]
23. Blasiak LC, Vaillancourt FH, Walsh CT, Drennan CL. Crystal structure of the non-haem iron halogenase SyrB2 in syringomycin biosynthesis. Nature. 2006; 440:368–371. [PubMed: 16541079]
24. Buongiorno D, Straganz GD. Structure and function of atypically coordinated enzymatic mononuclear non-heme-Fe(II) centers. Coord. Chem. Rev. 2013; 257:541–563. [PubMed: 24850951]
25. Burger RM, Peisach J, Horwitz SB. Activated Bleomycin - A Transient Complex of Drug, Iron, and Oxygen that Degrades DNA. J. Biol. Chem. 1981; 256:1636–1644. [PubMed: 6257682]
26. Spiro TG, Li X-Y. Resonance Raman spectroscopy of metalloporphyrins. Biol. Appl. Raman Spectrosc. 1988; 3:1–37.
27. Price JC, Barr EW, Tirupati B, Bollinger JM, Krebs C. The first direct characterization of a high-valent iron intermediate in the reaction of an alpha-ketoglutarate-dependent dioxygenase: A high-spin Fe(IV) complex in taurine/alpha-ketoglutarate dioxygenase (TauD) from Escherichia coli. Biochemistry. 2003; 42:7497–7508. [PubMed: 12809506]
28. Eser BE, Barr EW, Frantorn PA, Saleh L, Bollinger JM Jr, Krebs C, Fitzpatrick PF. Direct spectroscopic evidence for a high-spin Fe(IV) intermediate in tyrosine hydroxylase. J. Am. Chem. Soc. 2007; 129:11334–11335. [PubMed: 17715926]
29. Mbughuni MM, Chakrabarti M, Hayden JA, Bominaar EL, Hendrich MP, Muenck E, Lipscomb JD. Trapping and spectroscopic characterization of an Fe-III-superoxo intermediate from a nonheme mononuclear iron-containing enzyme. Proc. Natl. Acad. Sci. United States Am. 2010; 107:16788–16793.
30. Mbughuni MM, Chakrabarti M, Hayden JA, Meier KK, Dalluge JJ, Hendrich MP, Muenck E, Lipscomb JD. Oxy Intermediates of Homoprotocatechuate 2,3-Dioxygenase: Facile Electron Transfer between Substrates. Biochemistry. 2011; 50:10262–10274. [PubMed: 22011290]
31. Meier KK, Rogers MS, Kovaleva EG, Mbughuni MM, Bominaar EL, Lipscomb JD, Münck E. A Long-Lived FeIII-(Hydroperoxo) Intermediate in the Active H200C Variant of Homoprotocatechuate 2, 3-Dioxygenase: Characterization by Mössbauer, Electron Paramagnetic Resonance, and Density Functional Theory Methods. Inorg. Chem. 2015; 54:10269–10280. [PubMed: 26485328]
32. Kemsley JN, Mitic N, Zaleski KL, Caradonna JP, Solomon EI. Circular dichroism and magnetic circular dichroism spectroscopy of the catalytically competent ferrous active site of phenylalanine hydroxylase and its interaction with pterin cosubstrate. J. Am. Chem. Soc. 1999; 121:1528–1536.
33. Ohta T, Chakrabarty S, Lipscomb JD, Solomon EI. Near-IR MCD of the nonheme ferrous active site in naphthalene 1,2-dioxygenase: Correlation to crystallography and structural insight into the mechanism of Rieske dioxygenases. J. Am. Chem. Soc. 2008; 130:1601–1610. [PubMed: 18189388]
34. Loeb KE, Zaleski JM, Westre TE, Guajardo RJ, Mascharak PK, Hedman B, Hodgson KO, Solomon EI. Spectroscopic definition of the geometric and electronic structure of the non-heme iron active site in iron (II) bleomycin: Correlation with oxygen reactivity. J. Am. Chem. Soc. 1995; 117:4545–4561.
35. Davis MI, Wasinger EC, Decker A, Pau MY, Vaillancourt FH, Bolin JT, Eltis LD, Hedman B, Hodgson KO, Solomon EI. Spectroscopic and electronic structure studies of 2, 3-

dihydroxybiphenyl 1, 2-dioxygenase: O2 reactivity of the non-heme ferrous site in extradiol dioxygenases. J. Am. Chem. Soc. 2003; 125:11214–11227. [PubMed: 16220940]

36. Brown CD, Neidig ML, Neibergall MB, Lipscomb JD, Solomon EI. VTVH-MCD and DFT studies of thiolate bonding to {FeNO}(7)/{FeO2}(8) complexes of isopenicillin N synthase: Substrate determination of oxidase versus oxygenase activity in nonheme Fe enzymes. J. Am. Chem. Soc. 2007; 129:7427–7438. [PubMed: 17506560]
37. Zhou J, Kelly WL, Bachmann BO, Gunsior M, Townsend CA, Solomon EI. Spectroscopic studies of substrate interactions with clavaminate synthase 2, a multifunctional alpha-KG-dependent non-heme iron enzyme: Correlation with mechanisms and reactivities. J. Am. Chem. Soc. 2001; 123:7388–7398. [PubMed: 11472170]
38. Ryle MJ, Padmakumar R, Hausinger RP. Stopped-flow kinetic analysis of Escherichia coli taurine/α-ketoglutarate dioxygenase: interactions with α-ketoglutarate, taurine, and oxygen. Biochemistry. 1999; 38:15278–15286. [PubMed: 10563813]
39. Bollinger JM, Krebs C. Stalking intermediates in oxygen activation by iron enzymes: Motivation and method. J. Inorg. Biochem. 2006; 100:586–605. [PubMed: 16513177]
40. Ehrismann D, Flashman E, Genn DN, Mathioudakis N, Hewitson KS, Ratcliffe PJ, Schofield CJ. Studies on the activity of the hypoxia-inducible-factor hydroxylases using an oxygen consumption assay. Biochem. J. 2007; 401:227–234. [PubMed: 16952279]
41. Galonic DP, Barr EW, Walsh CT, Bollinger JM Jr, Krebs C. Two interconverting Fe((IV)) intermediates in aliphatic chlorination by the halogenase CytC3. Nat. Chem. Biol. 2007; 3:113–116. [PubMed: 17220900]
42. Panay AJ, Lee M, Krebs C, Bollinger JM Jr, Fitzpatrick PF. Evidence for a high-spin Fe (IV) species in the catalytic cycle of a bacterial phenylalanine hydroxylase. Biochemistry. 2011; 50:1928–1933. [PubMed: 21261288]
43. Hoffart LM, Barr EW, Guyer RB, Bollinger JM Jr, Krebs C. Direct spectroscopic detection of a C-H-cleaving high-spin Fe(IV) complex in a prolyl-4-hydroxylase. Proc. Natl. Acad. Sci. United States Am. 2006; 103:14738–14743.
44. Mantri M, Zhang Z, McDonough MA, Schofield CJ. Autocatalysed oxidative modifications to 2-oxoglutarate dependent oxygenases. FEBS J. 2012; 279:1563–1575. [PubMed: 22251775]
45. Valegard K, van Scheltinga ACT, Dubus A, Ranghino G, Oster LM, Hajdu J, Andersson I. The structural basis of cephalosporin formation in a mononuclear ferrous enzyme. Nat. Struct. & Mol. Biol. 2004; 11:95–101. [PubMed: 14718929]
46. Wójcik A, Radon M, Borowski T. Mechanism of O2 Activation by α-Ketoglutarate Dependent Oxygenases Revisited. A Quantum Chemical Study. J. Phys. Chem. 2016; 120:1261–1274.
47. Diebold AR, Brown-Marshall CD, Neidig ML, Brownlee JM, Moran GR, Solomon EI. Activation of alpha-Keto Acid-Dependent Dioxygenases: Application of an {FeNO}(7)/{FeO2}(8) Methodology for Characterizing the Initial Steps of O-2 Activation. J. Am. Chem. Soc. 2011; 133:18148–18160. [PubMed: 21981763]
48. Tarhonskaya H, Szollossi A, Leung IKH, Bush JT, Henry L, Chowdhury R, Iqbal A, Claridge TDW, Schofield CJ, Flashman E. Studies on deacetoxycephalosporin C synthase support a consensus mechanism for 2-oxoglutarate dependent oxygenases. Biochemistry. 2014; 53:2483–2493. [PubMed: 24684493]
49. Zhang ZH, Ren JS, Stammers DK, Baldwin JE, Harlos K, Schofield CJ. Structural origins of the selectivity of the trifunctional oxygenase clavaminic acid synthase. Nat. Struct. Biol. 2000; 7:127–133. [PubMed: 10655615]
50. Wasinger EC, Mitic N, Hedman B, Caradonna J, Solomon EI, Hodgson KO. X-ray absorption spectroscopic investigation of the resting ferrous and cosubstrate-bound active sites of phenylalanine hydroxylase. Biochemistry. 2002; 41:6211–6217. [PubMed: 12009881]
51. Light KM, Hangasky JA, Knapp MJ, Solomon EI. Spectroscopic Studies of the Mononuclear Non-Heme Fe-II Enzyme FIH: Second-Sphere Contributions to Reactivity. J. Am. Chem. Soc. 2013; 135:9665–9674. [PubMed: 23742069]
52. Saban E, Chen Y-H, Hangasky JA, Taabazuing CY, Holmes BE, Knapp MJ. The Second Coordination Sphere of FIH Controls Hydroxylation. Biochemistry. 2011; 50:4733–4740. [PubMed: 21456582]

53. Kumar D, Hirao H, Shaik S, Kozlowski PM. Proton-shuffle mechanism of O-O activation for formation of a high-valent oxo-iron species of bleomycin. J. Am. Chem. Soc. 2006; 128:16148–16158. [PubMed: 17165768]
54. Burger RM, Usov OM, Grigoryants VM, Scholes CP. Cryogenic photolysis of activated bleomycin to ferric bleomycin. J. Phys. Chem. B. 2006; 110:20702–20709. [PubMed: 17034262]
55. Liu LV, Bell CB III, Wong SD, Wilson SA, Kwak Y, Chow MS, Zhao J, Hodgson KO, Hedman B, Solomon EI. Definition of the intermediates and mechanism of the anticancer drug bleomycin using nuclear resonance vibrational spectroscopy and related methods. Proc. Natl. Acad. Sci. United States Am. 2010; 107:22419–22424.
56. Seto M, Yoda Y, Kikuta S, Zhang XW, Ando M. Observation of Nuclear Resonant Scattering Accompanied by Phonon Excitation Using Synchrotron Radiation. Phys. Rev. Lett. 1995; 74:3828–3831. [PubMed: 10058307]
57. Sturhahn W, Toellner TS, Alp EE, Zhang X, Ando M, Yoda Y, Kikuta S, Seto M, Kimball CW, Dabrowski B. Phonon Density-of-States Measured by Inelastic Nuclear Resonant Scattering. Phys. Rev. Lett. 1995; 74:3832–3835. [PubMed: 10058308]
58. Cooper HLR, Groves JT. Molecular probes of the mechanism of cytochrome P450. Oxygen traps a substrate radical intermediate. Arch. Biochem. Biophys. 2011; 507:111–118. [PubMed: 21075070]
59. Rittle J, Green MT. Cytochrome P450 Compound I: Capture, Characterization, and C-H Bond Activation Kinetics. Science. 2010; 330:933–937. [PubMed: 21071661]
60. Solomon EI, Wong SD, Liu LV, Decker A, Chow MS. Peroxo and oxo intermediates in mononuclear nonheme iron enzymes and related active sites. Curr. Opin. Chem. Biol. 2009; 13:99–113. [PubMed: 19278895]
61. Solomon EI, Decker A, Lehnert N. Non-heme iron enzymes: Contrasts to heme catalysis. Proc. Natl. Acad. Sci. United States Am. 2003; 100:3589–3594.
62. Chow MS, Liu LV, Solomon EI. Further insights into the mechanism of the reaction of activated bleomycin with DNA. Proc. Natl. Acad. Sci. United States Am. 2008; 105:13241–13245.
63. Decker A, Chow MS, Kemsley JN, Lehnert N, Solomon EI. Direct hydrogen-atom abstraction by activated bleomycin: An experimental and computational study. J. Am. Chem. Soc. 2006; 128:4719–4733. [PubMed: 16594709]
64. Stubbe J, Kozarich JW. Mechanisms of bleomycin-induced DNA degradation. Chem. Rev. 1987; 87:1107–1136.
65. Riggs-Gelasco PJ, Price JC, Guyer RB, Brehm JH, Barr EW, Bollinger JM, Krebs C. EXAFS spectroscopic evidence for an Fe O unit in the Fe (IV) intermediate observed during oxygen activation by taurine: α-ketoglutarate dioxygenase. J. Am. Chem. Soc. 2004; 126:8108–8109. [PubMed: 15225039]
66. Proshlyakov DA, Henshaw TF, Monterosso GR, Ryle MJ, Hausinger RP. Direct detection of oxygen intermediates in the non-heme Fe enzyme taurine/α-ketoglutarate dioxygenase. J. Am. Chem. Soc. 2004; 126:1022–1023. [PubMed: 14746461]
67. McDonald AR, Que L. High-valent nonheme iron-oxo complexes: Synthesis, structure, and spectroscopy. Coord. Chem. Rev. 2013; 257:414–428.
68. Fujimori DG, Barr EW, Matthews ML, Koch GM, Yonce JR, Walsh CT, Bollinger JM Jr, Krebs C, Riggs-Gelasco PJ. Spectroscopic evidence for a high-spin Br-Fe(IV)-Oxo intermediate in the alpha-ketoglutarate-dependent halogenase CytC3 from Streptomyces. J. Am. Chem. Soc. 2007; 129:13408–13409. [PubMed: 17939667]
69. Wong SD, Srnec M, Matthews ML, Liu LV, Kwak Y, Park K, Bell CB III, Alp EE, Zhao J, Yoda Y, Kitao S, Seto M, Krebs C, Bollinger JM Jr, Solomon EI. Elucidation of the Fe(IV)=O intermediate in the catalytic cycle of the halogenase SyrB2. Nature. 2013; 499:320–323. [PubMed: 23868262]
70. Srnec M, Wong SD, Matthews ML, Krebs C, Bollinger JM Jr, Solomon EI. Electronic Structure of the Ferryl Intermediate in the α-Ketoglutarate Dependent Non-Heme Iron Halogenase SyrB2: Contributions to H Atom Abstraction Reactivity. J. Am. Chem. Soc. 2016; 138:5110–5122. [PubMed: 27021969]
71. England J, Guo Y, Farquhar ER, Young VG Jr, Muenck E, Que L Jr. The Crystal Structure of a High-Spin Oxoiron(IV) Complex and Characterization of Its Self-Decay Pathway. J. Am. Chem. Soc. 2010; 132:8635–8644. [PubMed: 20568768]

72. England J, Martinho M, Farquhar ER, Frisch JR, Bominaar EL, Münck E, Que L. A Synthetic High-Spin Oxoiron (IV) Complex: Generation, Spectroscopic Characterization, and Reactivity. Angew. Chem. 2009; 121:3676–3680.

73. Srnec M, Wong SD, England J, Que L Jr, Solomon EI. pi-Frontier molecular orbitals in S=2 ferryl species and elucidation of their contributions to reactivity. Proc. Natl. Acad. Sci. United States Am. 2012; 109:14326–14331.

74. Choroba OW, Williams DH, Spencer JB. Biosynthesis of the vancomycin group of antibiotics: Involvement of an unusual dioxygenase in the pathway to (S)-4-hydroxyphenylglycine. J. Am. Chem. Soc. 2000; 122:5389–5390.

75. Johnson-Winters K, Purpero VM, Kavana M, Nelson T, Moran GR. (4-Hydroxyphenyl) pyruvate dioxygenase from Streptomyces avermitilis: the basis for ordered substrate addition. Biochemistry. 2003; 42:2072–2080. [PubMed: 12590595]

76. Neidig ML, Decker A, Choroba OW, Huang F, Kavana M, Moran GR, Spencer JB, Solomon EI. Spectroscopic and electronic structure studies of aromatic electrophilic attack and hydrogen-atom abstraction by non-heme iron enzymes. Proc. Natl. Acad. Sci. United States Am. 2006; 103:12966–12973.

77. Matthews ML, Neumann CS, Miles LA, Grove TL, Booker SJ, Krebs C, Walsh CT, Bollinger JM Jr. Substrate positioning controls the partition between halogenation and hydroxylation in the aliphatic halogenase, SyrB2. Proc. Natl. Acad. Sci. United States Am. 2009; 106:17723–17728.

78. Sono M, Roach MP, Coulter ED, Dawson JH. Heme-Containing Oxygenases. Chem. Rev. 1996; 96:2841–2888. [PubMed: 11848843]

79. Decker A, Rohde J-U, Klinker EJ, Wong SD, Que L Jr, Solomon EI. Spectroscopic and quantum chemical studies on low-spin Fe-IV=O complexes: Fe-O bonding and its contributions to reactivity. J. Am. Chem. Soc. 2007; 129:15983–15996. [PubMed: 18052249]

80. Roach PL, Clifton IJ, Hensgens CMH, Shibata N, Schofield CJ, Hajdu J, Baldwin JE. Structure of isopenicillin N synthase complexed with substrate and the mechanism of penicillin formation. Nature. 1997; 387:827–830. [PubMed: 9194566]

81. Kovaleva EG, Lipscomb JD. Crystal structures of Fe2+ dioxygenase superoxo, alkylperoxo, and bound product intermediates. Science. 2007; 316:453–457. [PubMed: 17446402]

82. Rivard BS, Rogers MS, Marell DJ, Neibergall MB, Chakrabarty S, Cramer CJ, Lipscomb JD. Rate-Determining Attack on Substrate Precedes Rieske Cluster Oxidation during Cis-Dihydroxylation by Benzoate Dioxygenase. Biochemistry. 2015; 54:4652–4664. [PubMed: 26154836]

83. Tamanaha EY, Zhang B, Guo Y, Chang W, Barr EW, Xing G, St. Clair J, Ye S, Neese F, Bollinger J, Martin J. Spectroscopic evidence for the two CH-cleaving intermediates of Aspergillus nidulans isopenicillin N synthase. J. Am. Chem. Soc. 2016

84. Vaillancourt FH, Barbosa CJ, Spiro TG, Bolin JT, Blades MW, Turner RFB, Eltis LD. Definitive evidence for monoanionic binding of 2,3-dihydroxybiphenyl to 2,3-dihydroxybiphenyl 1,2-dioxygenase from UV resonance Raman spectroscopy, UV/Vis absorption spectroscopy, and crystallography. J. Am. Chem. Soc. 2002; 124:2485–2496. [PubMed: 11890797]

85. Senda T, Sugiyama K, Narita H, Yamamoto T, Kimbara K, Fukuda M, Sato M, Yano K, Mitsui Y. Three-dimensional Structures of Free Form and Two Substrate Complexes of an Extradiol Ring-cleavage Type Dioxygenase, the BphC Enzyme from Pseudomonassp. Strain KKS102. J. Mol. Biol. 1996; 255:735–752. [PubMed: 8636975]

86. Mabrouk PA, Orville AM, Lipscomb JD, Solomon EI. Variable-temperature variable-field magnetic circular dichroism studies of the iron (II) active site in metapyrocatechase: implications for the molecular mechanism of extradiol dioxygenases. J. Am. Chem. Soc. 1991; 113:4053–4061.

87. Kita A, Kita S, Fujisawa I, Inaka K, Ishida T, Horiike K, Nozaki M, Miki K. An archetypical extradiol-cleaving catecholic dioxygenase: the crystal structure of catechol 2, 3-dioxygenase (metapyrocatechase) from Pseudomonas putida mt-2. Structure. 1999; 7:25–34. [PubMed: 10368270]

88. Wood PM. The potential diagram for oxygen at pH 7. Biochem. J. 1988; 253:287–289. [PubMed: 2844170]

89. Hagedoorn P-L, Schmidt PP, Andersson KK, Hagen WR, Flatmark T, Martínez A. The effect of substrate, dihydrobiopterin, and dopamine on the EPR spectroscopic properties and the midpoint

potential of the catalytic iron in recombinant human phenylalanine hydroxylase. J. Biol. Chem. 2001; 276:22850–22856. [PubMed: 11301319]

90. Schenk G, Pau MYM, Solomon EI. Comparison between the geometric and electronic structures and reactivities of {FeNO}(7) and {FeO2}(8) complexes: A density functional theory study. J. Am. Chem. Soc. 2004; 126:505–515. [PubMed: 14719948]
91. Roach PL, Clifton IJ, Fulop V, Harlos K, Barton GJ, Hajdu J, Andersson I, Schofield CJ, Baldwin JE. Crystal Structure of Isopenicillin N-Synthase is the First from a New Structural Family of Enzymes. Nature. 1995; 375:700–704. [PubMed: 7791906]
92. Lipscomb JD. Mechanism of extradiol aromatic ring-cleaving dioxygenases. Curr. Opin. Struct. Biol. 2008; 18:644–649. [PubMed: 19007887]
93. Siegbahn PEM, Haeffner F. Mechanism for catechol ring-cleavage by non-heme iron extradiol dioxygenases. J. Am. Chem. Soc. 2004; 126:8919–8932. [PubMed: 15264822]
94. Christian GJ, Ye S, Neese F. Oxygen activation in extradiol catecholate dioxygenases - a density functional study. Chem. Sci. 2012; 3:1600–1611.
95. Ferraro DJ, Gakhar L, Ramaswamy S. Rieske business: Structure-function of Rieske non-heme oxygenases. Biochem. Biophys. Res. Commun. 2005; 338:175–190. [PubMed: 16168954]
96. Neibergall MB, Stubna A, Mekmouche Y, Munck E, Lipscomb JD. Hydrogen peroxide dependent cis-dihydroxylation of benzoate by fully oxidized benzoate 1,2-dioxygenase. Biochemistry. 2007; 46:8004–8016. [PubMed: 17567152]
97. Karlsson A, Parales JV, Parales RE, Gibson DT, Eklund H, Ramaswamy S. Crystal structure of naphthalene dioxygenase: Side-on binding of dioxygen to iron. Science. 2003; 299:1039–1042. [PubMed: 12586937]
98. Ashikawa Y, Fujimoto Z, Usami Y, Inoue K, Noguchi H, Yamane H, Nojiri H. Structural insight into the substrate- and dioxygen-binding manner in the catalytic cycle of Rieske nonheme iron oxygenase system, carbazole 1,9a-dioxygenase. Bmc Struct. Biol. 2012; 12

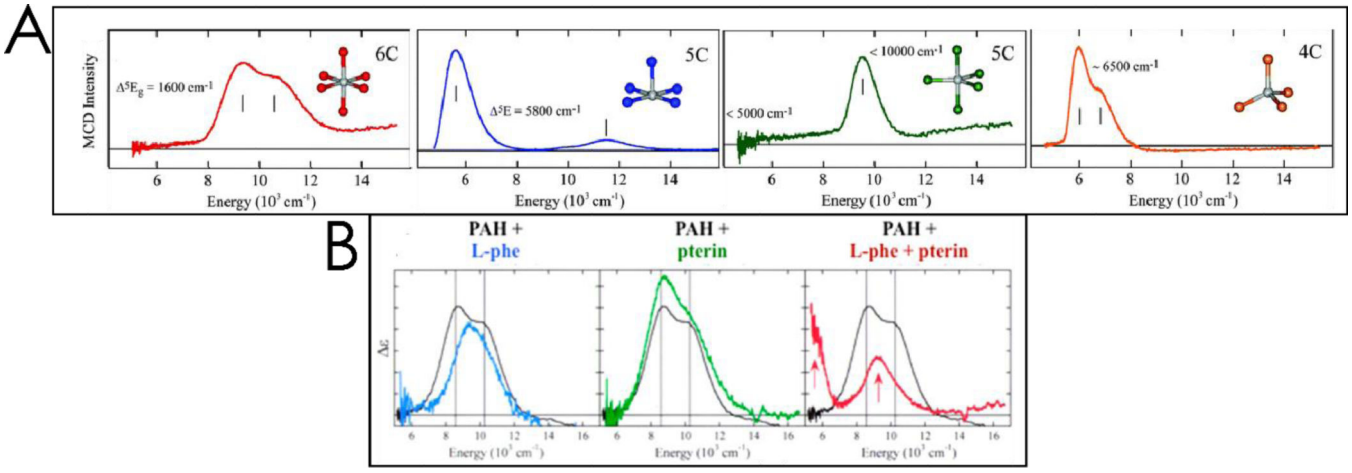

Figure 1.

Panel A: Representative low temperature MCD spectra for (from L to R) 6C octahedral, 5C square pyramidal, 5C trigonal bipyramidal, and 4C distorted tetrahedral non-heme Fe (NHFe) complexes. Panel B: MCD spectra for resting PAH (black) overlaid with spectra for (from L to R) PAH-L-Phe (blue), PAH-pterin (green), and PAH-L-Phe-pterin (red). Only coordination of both cosubstrates leads to a 5C site. Adapted from ref 2.

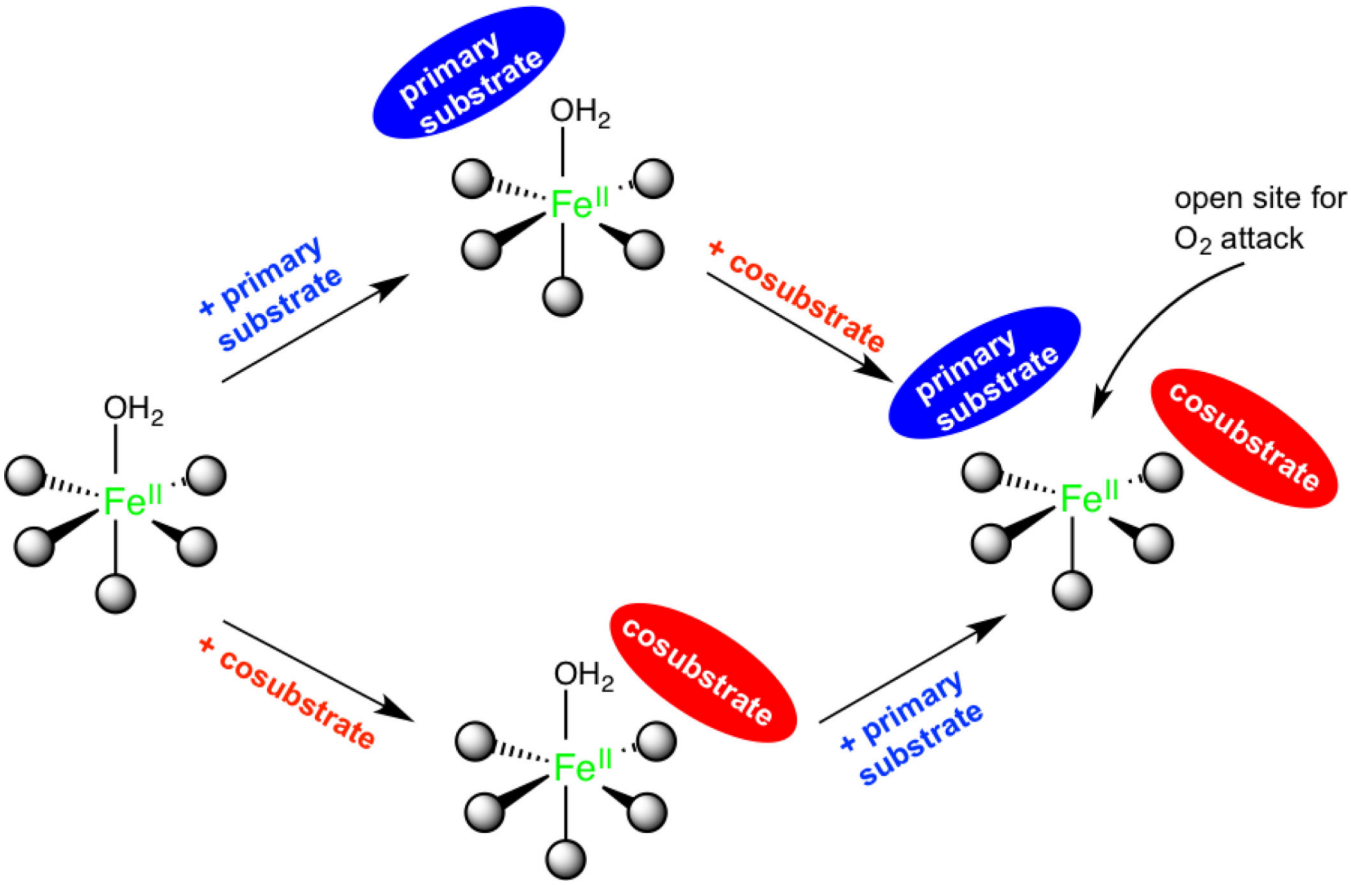

Figure 2.

The general mechanistic strategy for NHFe enzymes, where a coordination position for O_2 is only available when all cosubstrates are bound to the active site. Adapted from ref 2.

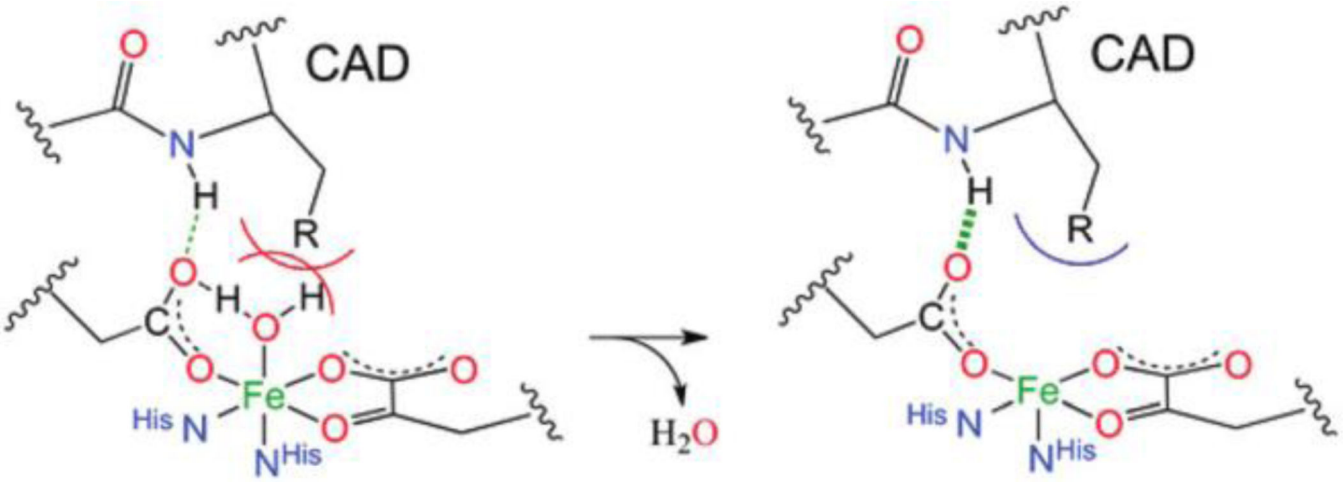

Figure 3.

Schematic showing the H-bonding and steric contributions to water loss and 5C site formation in FIH upon substrate (C- terminal transactivation domain, CAD) binding. Adapted from ref 51.

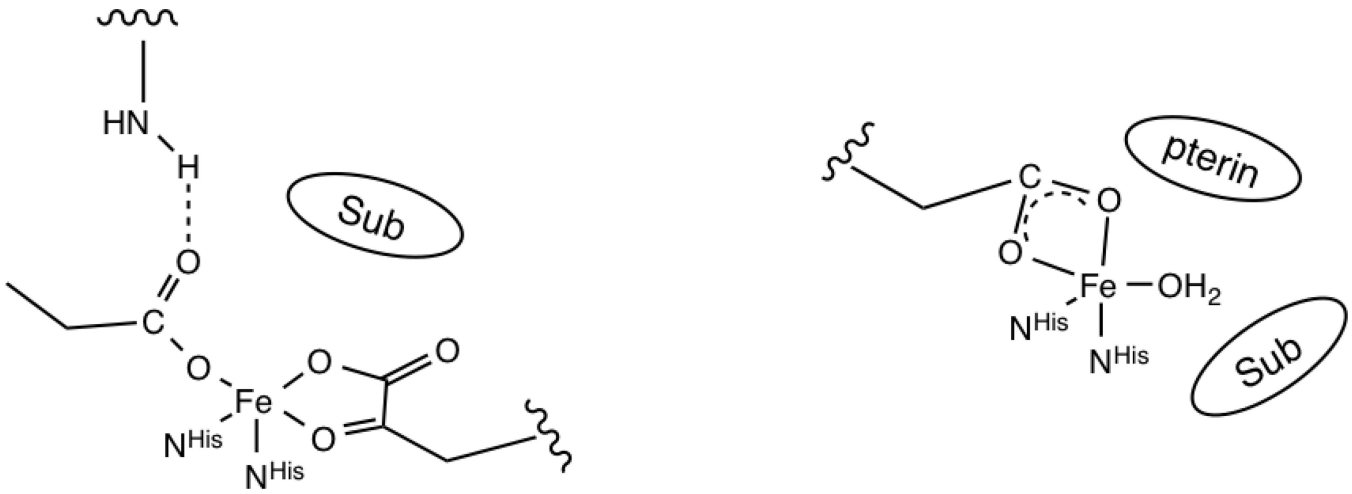

Figure 4.

Schematic comparison of facial triad coordination for the classes of NHFe enzymes that have a second-sphere residue hydrogen bonding to the coordinated carboxylate (αKG dependent enzymes, shown at left, and the extradiol dioxygenases), leading to monodentate coordination, and those without a hydrogen bonding residue (pterin dependent enzymes, shown at right, and the Rieske dioxygenases), which leads to bidentate carboxylate coordination.

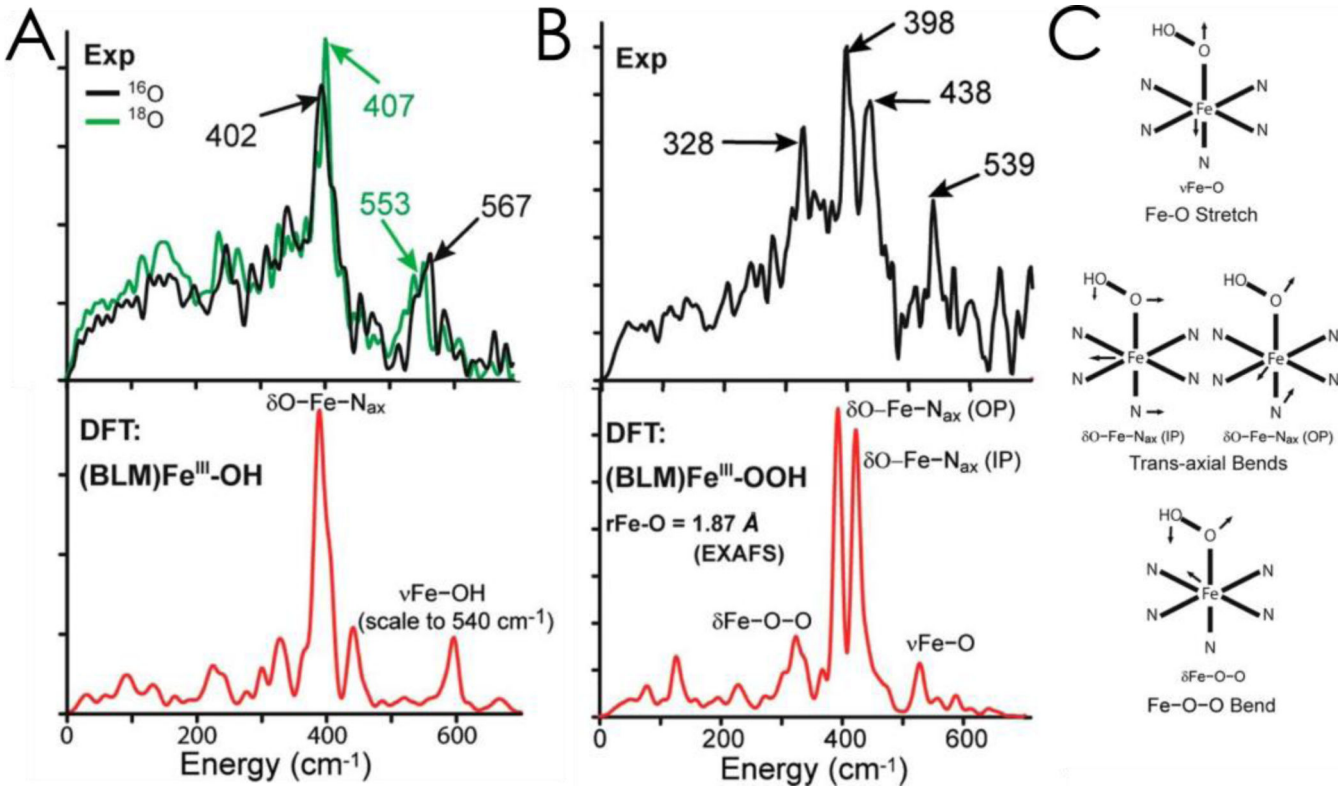

Figure 5.

A: NRVS spectra (top) and simulations (bottom) for low-spin ferric BLM showing an axial hydroxide bound to the Fe. B: NRVS data (top) and simulations (bottom) for ABLM. The three-peak pattern in the data can only be modeled by a low-spin Fe^{III}-OOH structure. C: Schematic depictions of vibrations assigned in B. Adapted from ref 55.

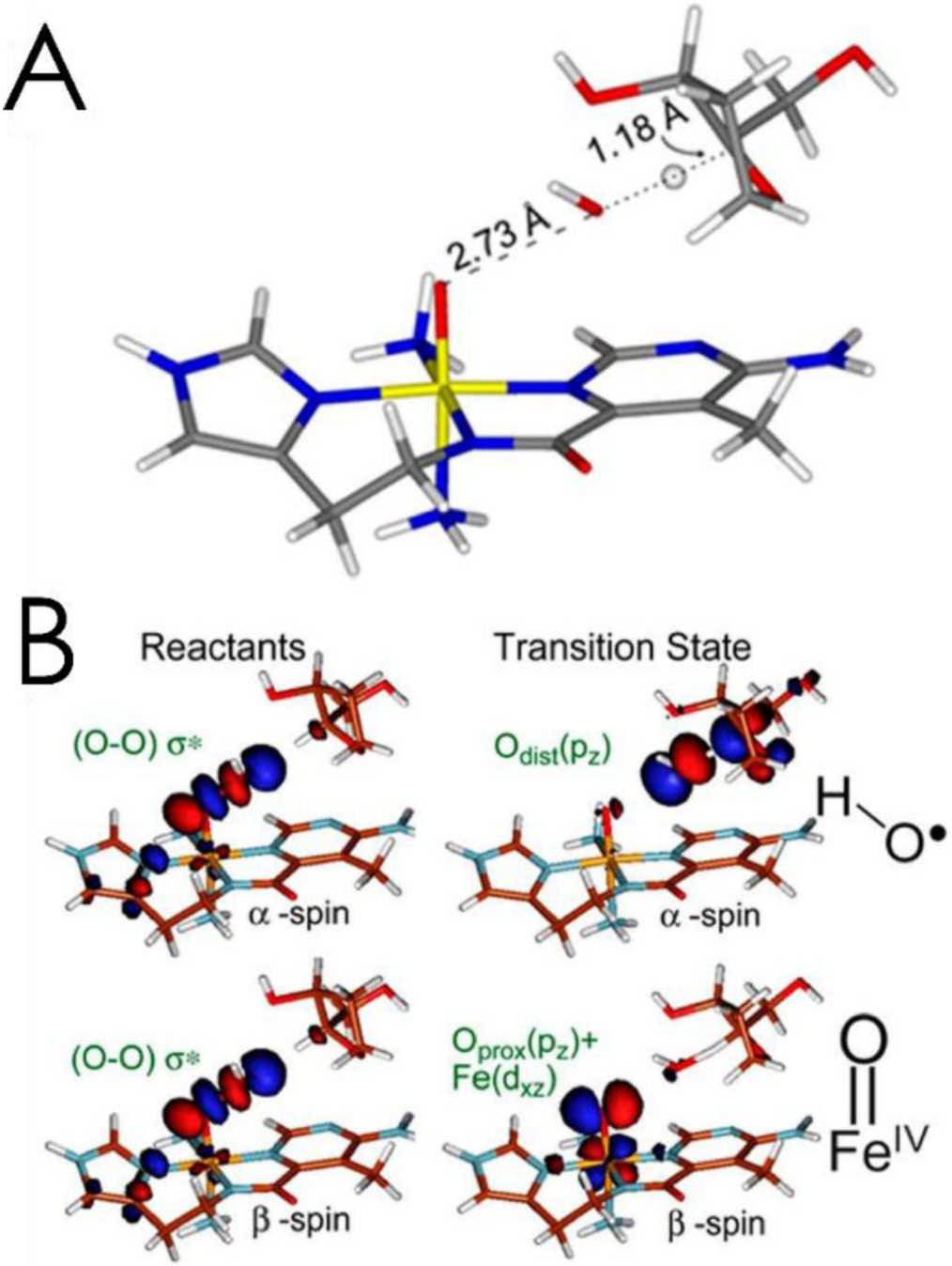

Figure 6.

A: Transition state for the direct H-atom abstraction of a proton by ABLM, which is late in O-O cleavage and early in C-H abstraction. B: The hydroperoxo σ* FMO of the low-spin ABLM reactant (left), which polarizes into a hydroxyl radical and Fe^{IV}=O at the transition state (right). Adapted from ref 63.

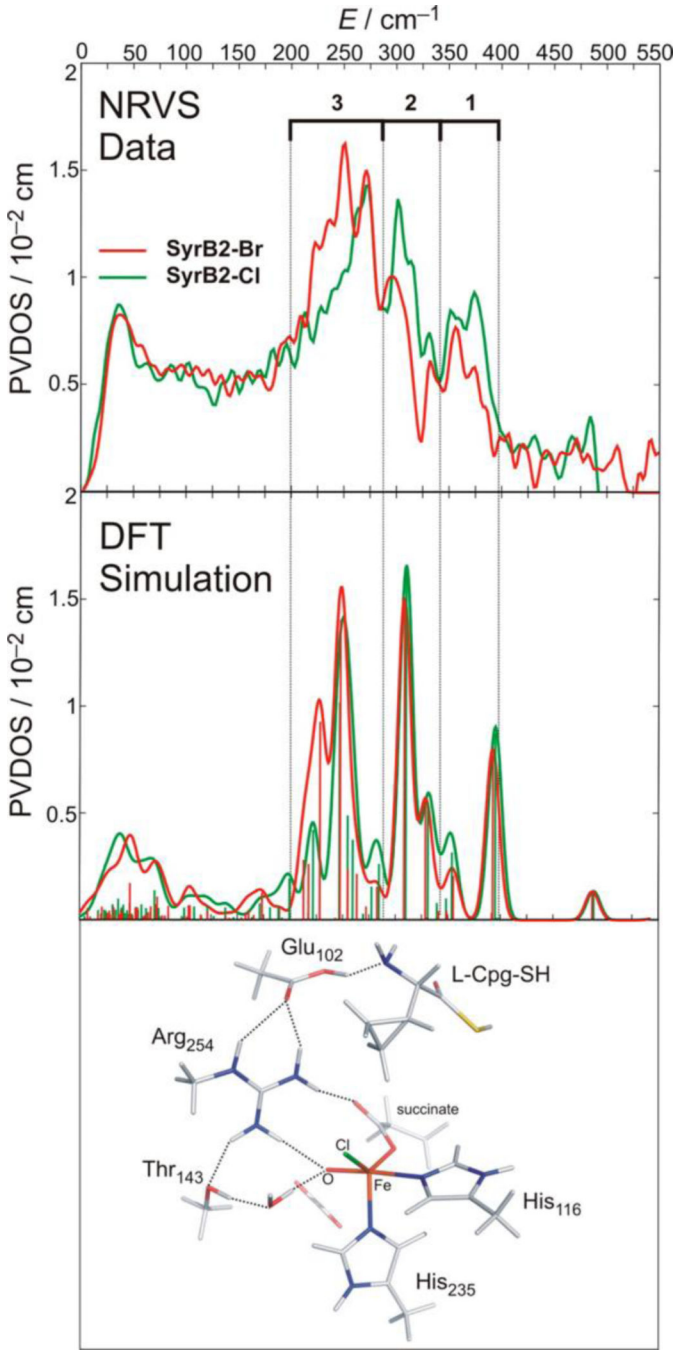

Figure 7.

Top: NRVS spectra for SyrB2-Cl (green) and SyrB2-Br (red). Middle: DFT NRVS simulations derived from the structure that best reproduces the experimental data. Bottom: Experimentally derived structure of the Fe^{IV}=O intermediate of SyrB2, which has a 5C trigonal bipyramidal geometry and an ~C_3 axis. Adapted from ref 69.

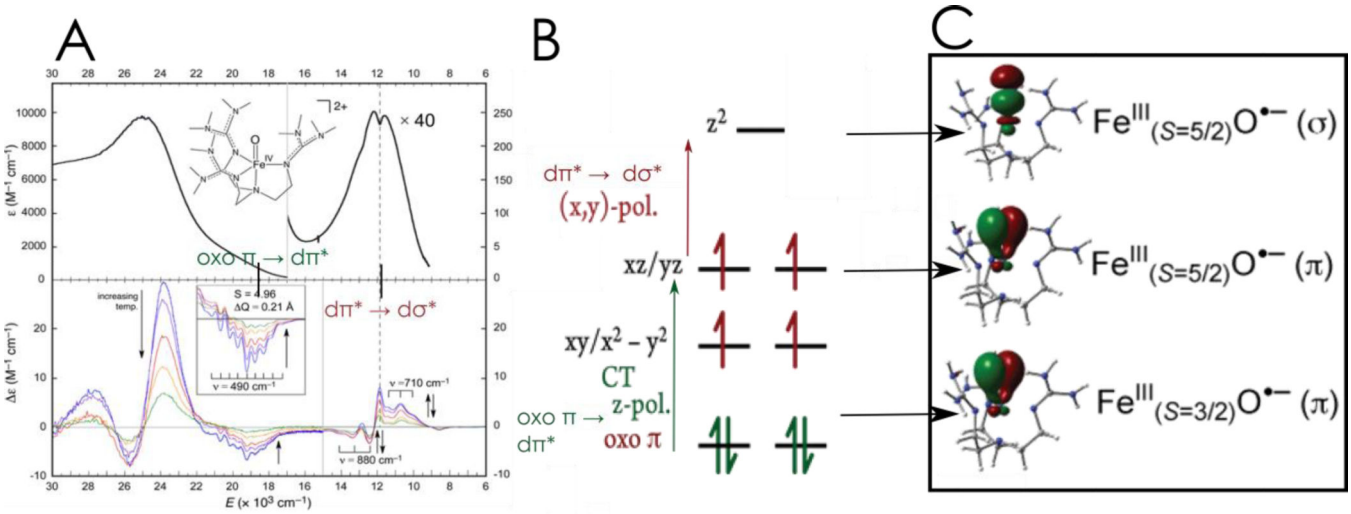

Figure 8.

A: Absorption (top) and MCD data (bottom) for $[Fe^{IV}(O)(TMG_3tren)]^{2+}$. B: LF and CT transitions of $[Fe^{IV}(O)(TMG_3tren)]^{2+}$ C: FMOs of $[Fe^{IV}(O)(TMG_3tren)]^{2+}$ at the transition state demonstrating Fe^{III}-$O^{\bullet-}$ character and the different channels for reactivity. Adapted from ref 73.

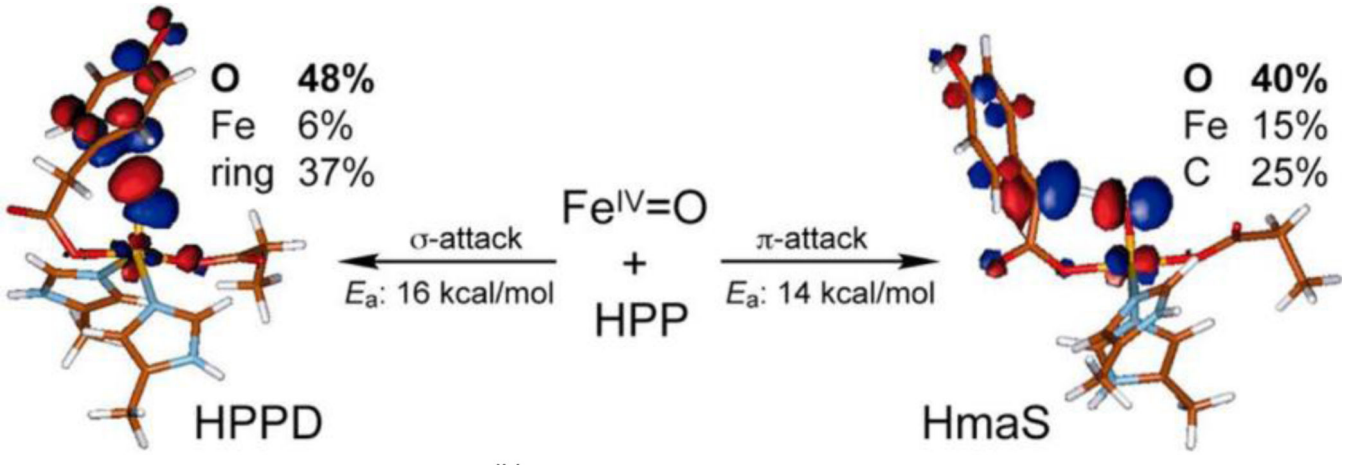

Figure 9.

FMOs of the Fe^{IV}=O intermediate in HPPD (left) and HmaS (right), demonstrating that different substrate orientations lead to different reactivities using different FMOs. Adapted from ref 76.

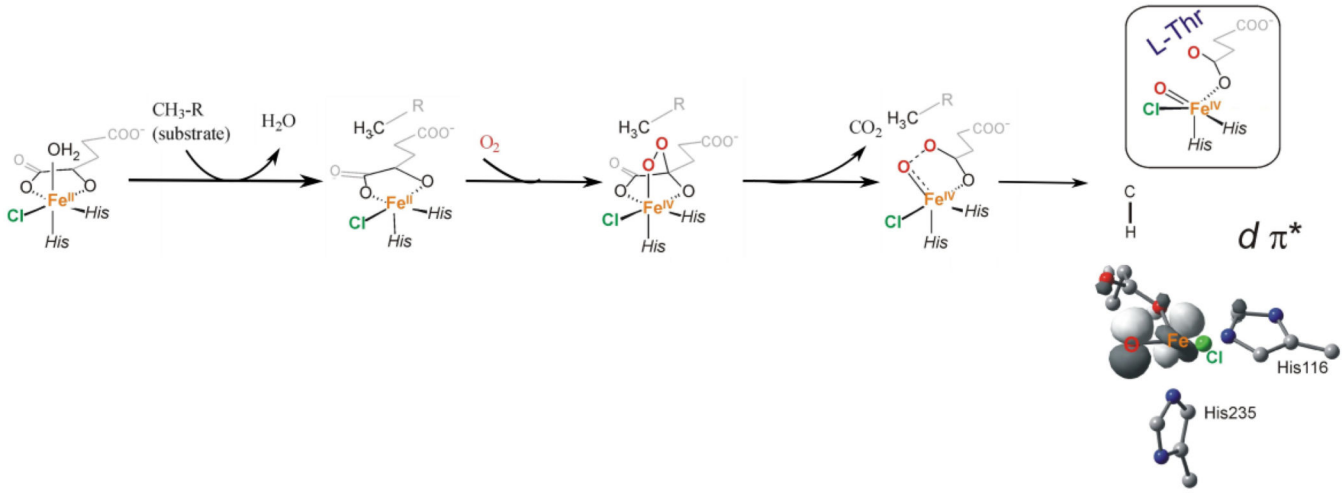

Figure 10.

Reaction coordinate for O_2 activation of SyrB2, leading to a 5C trigonal bipyramidal Fe^{IV}=O intermediate (as in Figure 7) with an Fe-O bond perpendicular to the substrate C-H bond. The contour gives the **π*** FMO used for reactivity. Adapted from ref 70.

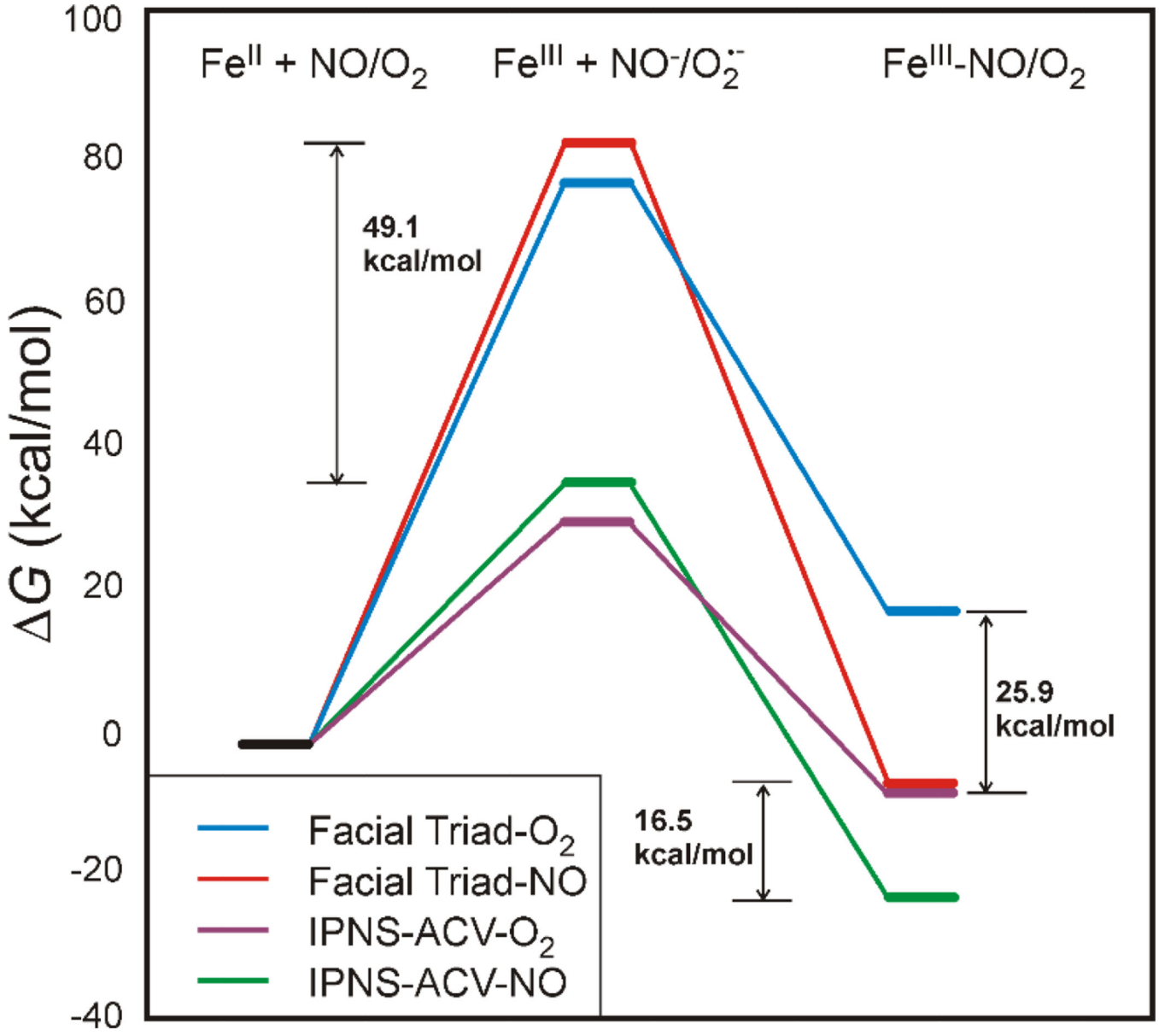

Figure 11.

Comparison of the free energies for the one-electron reduction of NO/O_2 by Fe^{II} (middle) and for the formation of a Fe^{III}-NO/O_2 complex (right) for a resting facial triad and for substrate-bound IPNS. Sulfur donation stabilizes formation of an Fe^{III}-O_2^- complex by 25.9 kcal/mol relative to a resting facial triad. Adapted from ref 36.

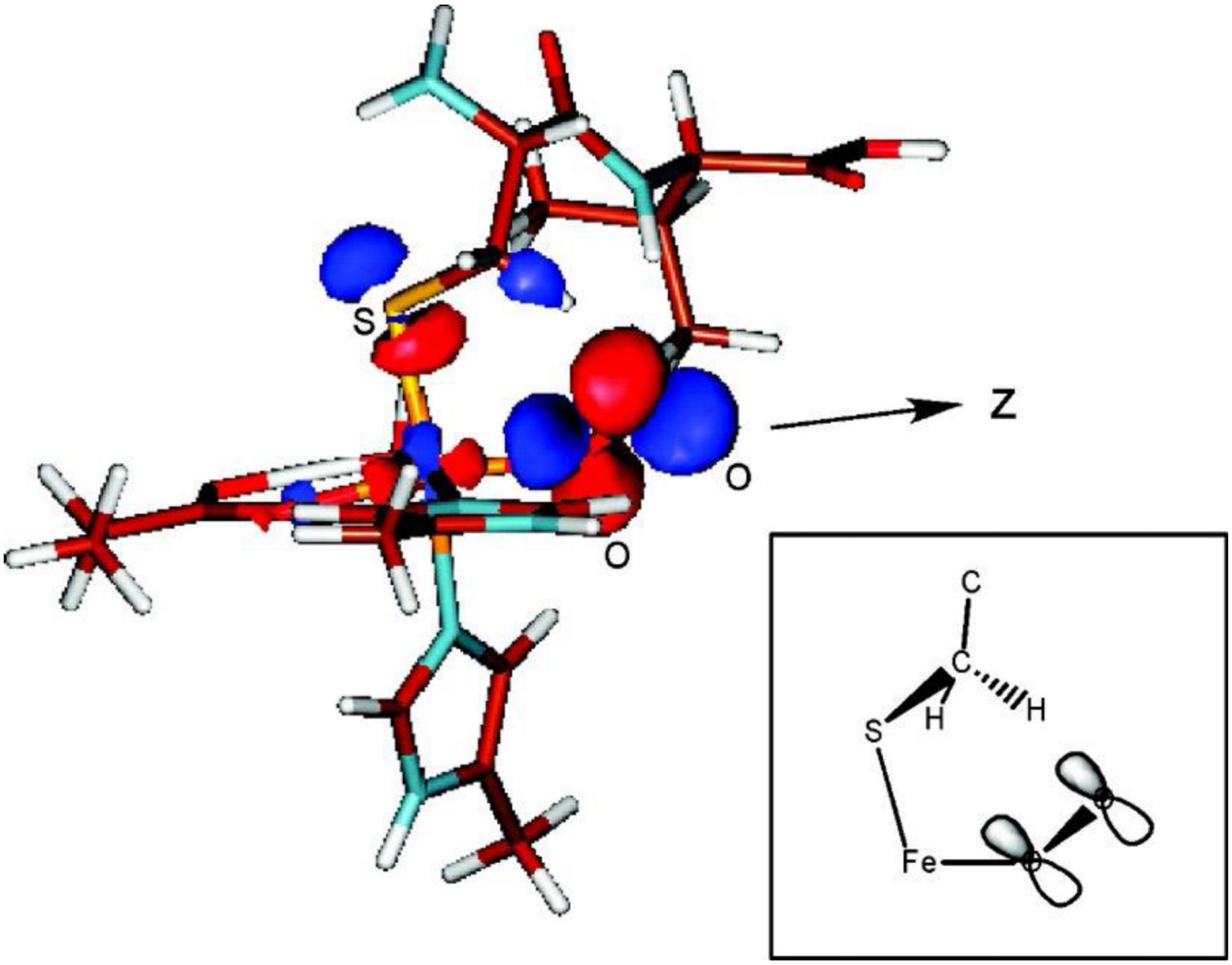

Figure 12.

FMO of Fe^{III}-ACV-O_2. Inset: Schematic of the unoccupied FMO, showing its favorable orientation for H-atom abstraction from the substrate β methylene carbon. Adapted from ref 36.

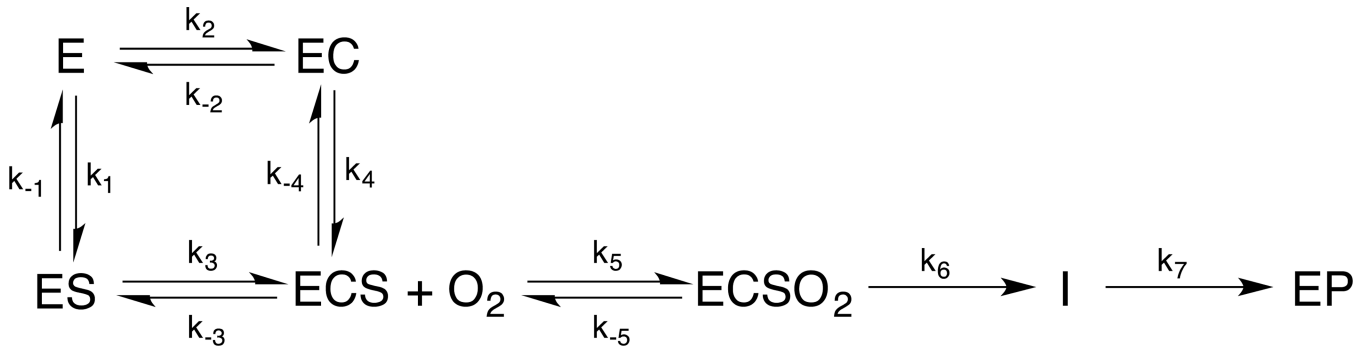

Scheme 1.

Kinetic model including the general mechanistic strategy in the αKG dependent dioxygenases

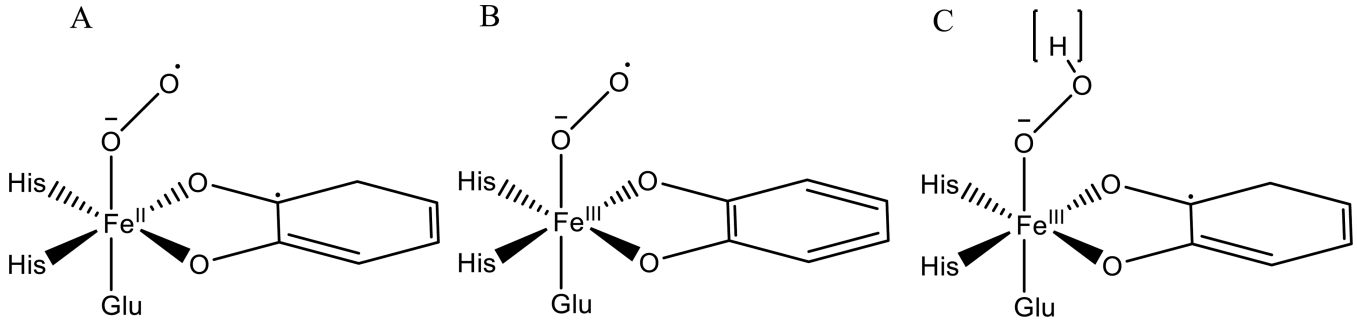

Scheme 2.

Possible electronic structures for the activated Fe-O_2 species in the extradiol dioxygenases.

Table 1

The classes of oxygen- and organic substrate-activating mononuclear non-heme Fe enzymes. Adapted from ref 2.